Fe-doping induced suppression of the second magnetic transition in $Sr_4Ru_3O_{10}$

Yan Liu,[1,2,3] Weiwei Chu,[2] Yu Wang,[4,6] Jiyong Yang,[2,5,*] Haifeng Du,[2] Wei Ning,[2] Zhe Qu,[2] Peigang Li,[4] Zhuan Xu,[1,7] Zhiqiang Mao,[4,6] and Mingliang Tian[2,7,†]

[1]*State Key Lab of Silicon Materials and Department of Physics, Zhejiang University, Hangzhou 310027, China*
[2]*Anhui Province Key Laboratory of Condensed Matter Physics at Extreme Conditions, High Magnetic Field Laboratory, Chinese Academy of Sciences, Hefei 230031, Anhui, China*
[3]*College of Physics and Electronic Engineering, Sichuan Normal University, Chengdu 610068, China*
[4]*Department of Physics and Engineering Physics, Tulane University, New Orleans, Louisiana 70118, USA*
[5]*School of Physical Science and Technology, Southwest University, Chongqing 400715, China*
[6]*Department of Physics, Pennsylvania State University, University Park, Pennsylvania 16802, USA*
[7]*Collaborative Innovation Center of Advanced Microstructures, Nanjing University, Nanjing 210093, China*

(Received 3 October 2018; revised manuscript received 4 April 2019; published 12 June 2019)

Ruthenium oxide ($Sr_4Ru_3O_{10}$) exhibits a second magnetic transition at a temperature T_M below its ferromagnetic (FM) transition ($T_C \sim 105$ K), which has attracted considerable attention in the past two decades. Here, we successfully grew $Sr_4(Ru_{1-x}Fe_x)_3O_{10}$ ($x = 0.01$) crystal and systematically investigated the magnetotransport property of its nanosheets. We found a feature that there is an in-plane FM order aligned along ⟨110⟩ directions below T_C without the occurrence of the second magnetic transition at T_M, which is in contrast to that expected in pure $Sr_4Ru_3O_{10}$ nanosheets, where the in-plane FM order will rotate to the c direction below T_M. Furthermore, a metamagnetic-like transition is also observed below ~50 K at about 2 T when the magnetic field is applied along the c axis. These results unambiguously demonstrate that the second magnetic transition at T_M is actually a consequence of spin reorientation induced by the inherent coupling between the spin and lattice, which can be effectively tuned by element doping.

DOI: 10.1103/PhysRevB.99.214418

I. INTRODUCTION

Ruddlesden-Popper (RP) series of ruthenium oxides [$Sr_{n+1}Ru_nO_{3n+1}$ ($n = 1, 2, \infty$)] are interesting materials displaying p-wave superconductivity (Sr_2RuO_4, $n = 1$) [1], field-tuned quantum criticality ($Sr_3Ru_2O_7$, $n = 2$) [2], and itinerant ferromagnetism ($SrRuO_3$, $n = \infty$) [3]. The $n = 3$ member, $Sr_4Ru_3O_{10}$, is an exotic ferromagnet with a Curie temperature $T_C \sim 105$ K, where the easy axis is along the c direction [4,5]. Its ferromagnetic (FM) transition is followed by a second magnetic transition at a temperature $T_M \sim 50-70$ K, below which a metamagnetic transition, i.e., a steep increase of magnetization near a critical magnetic field, is observed when an in-plane H is applied [4–7].

The nature of the second transition at T_M has been a long-lasting controversy. For instance, the magnetization and Raman spectra measurements suggest that this transition might be a FM to antiferromagnetic (AFM)-like transition in the ab plane [5,8], while no thermal anomaly is observed at T_M on the specific heat experiments [9,10]. A neutron diffraction experiment performed by Granata *et al.* [11] showed that the magnetic moments are only FM coupled along the c-axis with neither FM nor AFM component in the ab plane. However, a very recent neutron diffraction study by Zhu *et al.* [12] found that there are both in-plane and out-of-plane FM components, and below T_M the in-plane component inclines continuously toward the out-of-plane direction.

To understand the origin of the second transition at T_M we performed systematic transport studies on single crystalline $Sr_4Ru_3O_{10}$ nanosheets recently [13–16]. We found that T_M in nanosheets decreases with decreasing thickness and the FM order is within in the ab plane with magnetic moments along the ⟨110⟩ directions for $T_M < T < T_C$ [14–16], but below T_M, the in-plane FM order magically transforms to the c direction spontaneously [16]. We attributed this spin reorientation observed in $Sr_4Ru_3O_{10}$ nanosheets to the competition between the shape anisotropy and the inherent magnetocrystalline anisotropy, where the shape anisotropy increases with decreasing thickness and favors spins aligned in the ab plane, while the magnetocrystalline anisotropy favors spins aligned along the c direction [14,16], and hence it is possibly enhanced substantially at low temperatures due to the slight negative thermal expansion of the c axis near the bulk T_M [11,17].

Element doping is an effective way in tuning lattice parameters and thus provides possibility in tuning the magnetocrystalline anisotropy. Here, we successfully grew $Sr_4(Ru_{1-x}Fe_x)_3O_{10}$ ($x = 0.01$) (nominal concentration) single crystal using the floating-zone technique [18], and investigated the magnetism of its bulk and nanosheet. Since a 0.12% shrinking of the c axis by Fe-doping at room temperature is observed [Fig. 1(a)], the intrinsic magnetocrystalline anisotropy is therefore expected to be reduced accordingly, and thus leading to a suppression of the c axis FM order. Indeed, four distinct features are observed: (i) magnetization

*jyyang@hmfl.ac.cn
†tianml@hmfl.ac.cn

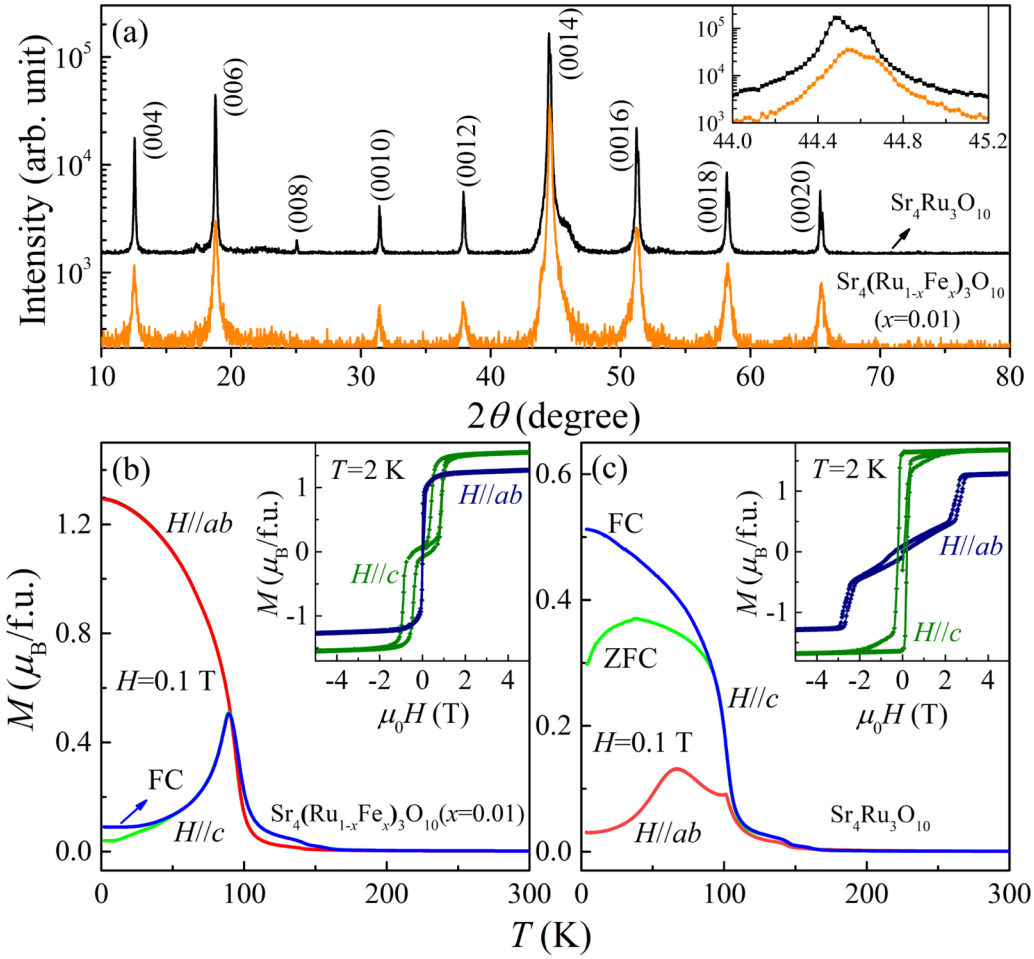

FIG. 1. (a) XRD patterns of a cleaved (001) surface of $Sr_4(Ru_{1-x}Fe_x)_3O_{10}$ ($x = 0.01$) (orange-line) and $Sr_4Ru_3O_{10}$ (black-line) crystals, grown by floating-zone method. Inset shows the most intensity (0014) peak. Data is shifted vertically for clarity. Panels (b) and (c) are, respectively, the magnetization M as functions of temperature T and magnetic field H (inset, 2 K) of a $Sr_4(Ru_{1-x}Fe_x)_3O_{10}$ ($x = 0.01$) single crystal and a pure $Sr_4Ru_3O_{10}$ single crystal.

measurement on the bulk shows that the magnetic easy direction has been changed from the c axis to the ab plane due to Fe-doping; (ii) only one resistive anomaly at ∼105 K due to the FM transition in $Sr_4(Ru_{1-x}Fe_x)_3O_{10}$ ($x = 0.01$) nanosheets is found, the second resistive anomaly, which occurs at T_M in pure $Sr_4Ru_3O_{10}$ bulk or nanosheets [5,6,13], is absent; (iii) the $Sr_4(Ru_{1-x}Fe_x)_3O_{10}$ ($x = 0.01$) nanosheet shows an in-plane FM order aligned along ⟨110⟩ directions in all temperature range below T_C; (iv) the anomalous Hall effect (AHE) with H applied along the c axis in the $Sr_4(Ru_{1-x}Fe_x)_3O_{10}$ ($x = 0.01$) nanosheet reveals that there is a metamagneticlike transition at about 2 T below ∼50 K, which is in contrast to the metamagnetic transition expected in the ab plane of the pure system. Our results suggest that replacing Ru with a few Fe ions favors magnetic moments aligned in the ab plane, which highlight the coupling effect between the lattice and spin in the $Sr_4Ru_3O_{10}$ system at temperatures below T_C.

II. EXPERIMENTS

Single crystals of $Sr_4(Ru_{1-x}Fe_x)_3O_{10}$ ($x = 0.01$) were grown by the floating zone method, which is similar to that described in Ref. [18], where the concentration of Fe was analyzed roughly by energy dispersive spectrum (EDS, Oxford instruments). The starting materials were $SrCO_3$ (99.99% purity), Fe_2O_3 (99.99%) and RuO_2 (99.95% purity). 25% excess RuO_2 was added to compensate the evaporation of RuO_2 from melting zone. The mixed powder was grinded for ∼1 h, and then pressed to pellets, after that the pellets were sintered at temperature of 900 °C for 12 h. The sintered pellets were grinded for ∼1 h again, the grinded powder was pressed to rod, and sintered at temperature of 1350 °C for 4 h. The growth speed was ∼15 mm/h and the pressure in quartz tube was ∼10 bar (10% O_2 + 90% Ar).

The structural property of the synthetic crystal was studied by a room temperature x-ray diffractometer (XRD) [Fig. 1(a)]. The magnetization of the $Sr_4(Ru_{1-x}Fe_x)_3O_{10}$ ($x = 0.01$) single crystal, which structure was verified firstly by XRD, was measured by a superconducting quantum interference device (SQUID) magnetometer [Fig. 1(b)].

$Sr_4(Ru_{1-x}Fe_x)_3O_{10}$ ($x = 0.01$) nanosheets were obtained by the scotch tape-based micro-mechanical exfoliation method from the bulk crystal. Nanosheets with different thicknesses, d, determined by atomic force microscopy were transferred onto a SiO_2 (300 nm)/Si substrate. Contacts were patterned using an electron-beam lithography technique

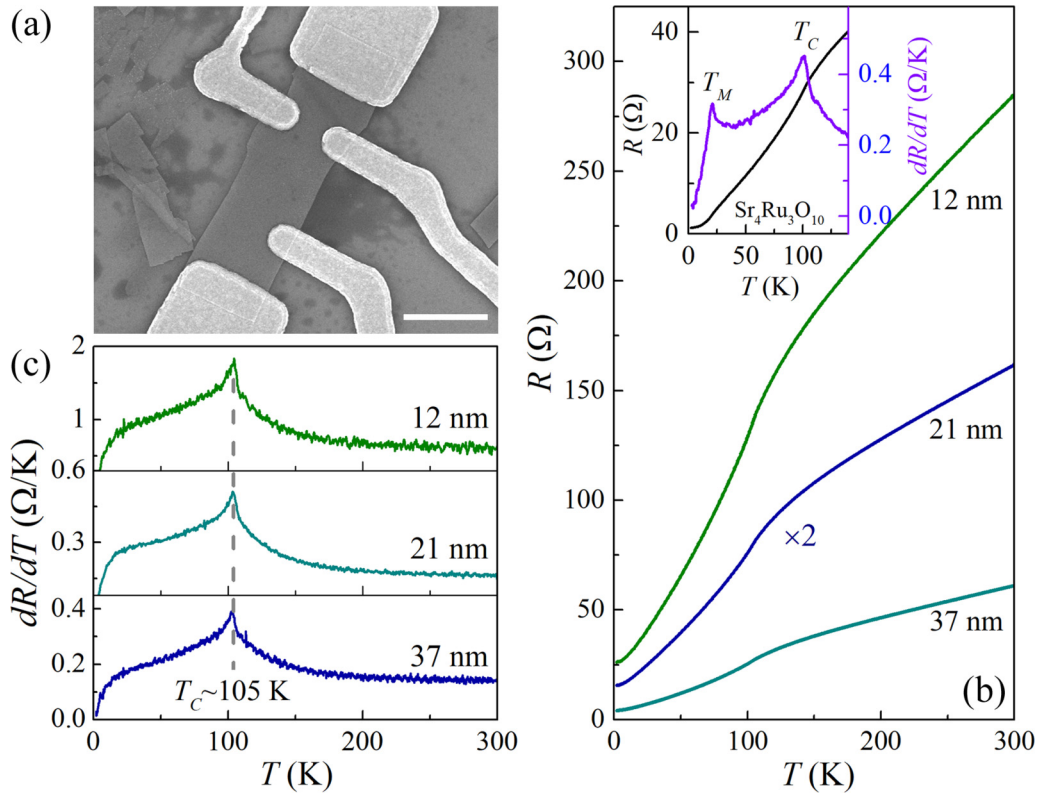

FIG. 2. (a) SEM image of a 12-nm-thick $Sr_4(Ru_{1-x}Fe_x)_3O_{10}$ ($x = 0.01$) nanosheet with patterned electrodes. Scale bar: 2 μm. Panels (b) and (c) are, respectively, the temperature T dependent zero-field resistance R and dR/dT of three $Sr_4(Ru_{1-x}Fe_x)_3O_{10}$ ($x = 0.01$) nanosheets with thickness of 12, 21, and 37 nm. Inset in (b): R and dR/dT versus T curves of a 34-nm-thick pure $Sr_4Ru_3O_{10}$ nanosheet. Two resistive anomalies at $T_C \sim 105$ K and $T_M \sim 25$ K can be identified.

followed by deposition of Ti/Au (5 nm/100 nm). The scanning electron microscope (SEM) image of a device with patterned electrodes is shown in Fig. 2(a). The transport property measurements of the nanosheets were carried out in a physical property measurement system (PPMS, Quantum Design). The Hall resistance R_{xy} is determined from $R_{xy} = [R_{xy}(H) - R_{xy}(-H)]/2$ to subtract the component of the longitudinal resistance arising from the small misalignment of transverse contacts.

III. RESULTS AND DISCUSSION

A. Structure and magnetization of bulk crystal

Figure 1(a) shows the XRD pattern taken on a cleaved (001) surface of the $Sr_4(Ru_{1-x}Fe_x)_3O_{10}$ ($x = 0.01$) crystal. For comparison, the XRD pattern of a pure $Sr_4Ru_3O_{10}$ crystal grown by the same method is also presented. One can find that the synthetic crystal well matches with the $Sr_4Ru_3O_{10}$ phase without other phases such as $Sr_3Ru_2O_7$ and $SrRuO_3$, indicating our $Sr_4(Ru_{1-x}Fe_x)_3O_{10}$ ($x = 0.01$) crystal is high-quality.

Since the ionic size of Fe is smaller than that of Ru, one will expect a shrinkage of the c axis correspondingly by Fe-doping [19]. Indeed, our XRD measurement shows that the lattice constant c of the $Sr_4(Ru_{1-x}Fe_x)_3O_{10}$ ($x = 0.01$) single crystal is about 0.12% shorter than that of the pure $Sr_4Ru_3O_{10}$ single crystal, determined from the most intensity (0014) peak [the inset of Fig. 1(a)].

Figure 1(b) shows the temperature T dependence of the magnetization M of a $Sr_4(Ru_{1-x}Fe_x)_3O_{10}$ ($x = 0.01$) single crystal measured with a magnetic field of $H = 0.1$ T and different cooling histories [zero field cooling (ZFC) and field cooling (FC)]. The magnetization of a pure $Sr_4Ru_3O_{10}$ single crystal grown by the same method is also presented in Fig. 1(c). M-T curve for $H \| ab$ shows a T_C of about ~100 K without distinct irreversibility [Fig. 1(b)]. However, M for $H \| c$ exhibits only a pronounced peak near T_C followed by clearly irreversibility below ~40 K. Both are completely different compared with the pure $Sr_4Ru_3O_{10}$ [Fig. 1(c)]. The inset of Fig. 1(b) shows the magnetization M as a function of magnetic field H measured at $T = 2$ K. For $H \| ab$, $Sr_4(Ru_{1-x}Fe_x)_3O_{10}$ ($x = 0.01$) presents typical FM behavior, as that of pure $Sr_4Ru_3O_{10}$ with $H \| c$ [inset of Fig. 1(c)]; whereas for $H \| c$, the moment of $Sr_4(Ru_{1-x}Fe_x)_3O_{10}$ ($x = 0.01$) shows an abrupt increase at ~0.8 T with clearly hysteresis when H is swept down, resembling the metamagnetic transition observed in pure $Sr_4Ru_3O_{10}$ with $H \| ab$ [inset of Fig. 1(c)] [5]. Besides, the saturation magnetization for $Sr_4(Ru_{1-x}Fe_x)_3O_{10}$ ($x = 0.01$) with $H \| ab$ (or $H \| c$) is almost the same with that of the pure $Sr_4Ru_3O_{10}$ with $H \| c$ (or $H \| ab$). These results show clearly that the magnetic easy direction has been changed from the c axis to the ab plane by Fe-doping, though the shrinkage of c here is only 0.12%, indicating a close relation between the lattice and spin in the $Sr_4Ru_3O_{10}$ system.

It should be pointed out here that, the structure property of the single crystal used in the magnetization measurement was verified firstly by single-crystal XRD as shown in Fig. 1(a), but a small increase of magnetization at ∼150 K is still observed, which indicates that there is very likely a small amount of $SrRuO_3$ phase in the crystal. The intergrowth is a common problem in synthesizing high-purity large ruthenate single crystals. To make our results more reliable, we use nanosheet rather than bulk to a deep investigation of its magnetic property. For nanosheets with a few tens nanometer in thickness, this intergrowth problem can be avoided effectively. This is because different phases in the $Sr_{n+1}Ru_nO_{3n+1}$ family have completely different *R-T* properties compared with $Sr_4Ru_3O_{10}$ [see, for example: Ref. [20] ($Sr_3Ru_2O_7$); Ref. [6] ($Sr_4Ru_3O_{10}$); Ref. [3] ($SrRuO_3$)]. Any other phases in nanosheet samples will give comparable contribution in transport and thus exhibit very different *R-T* behavior. We choose nanosheet samples with significant anomaly near $T_C \sim$ 100 K for further study, to ensure that our results are obtained on high purity samples.

B. Electrical resistance of nanosheet

Figure 2(b) shows the *T*-dependent longitudinal resistance *R* measured at zero magnetic field of three $Sr_4(Ru_{1-x}Fe_x)_3O_{10}$ ($x = 0.01$) nanosheets with thickness of 12, 21, and 37 nm, respectively. All *R-T* curves present very similar metallic behavior, accompanied by a resistive anomaly near $T_C \sim 105$ K, which can be more clearly identified from the "λ"-shaped dR/dT-*T* plot shown in Fig. 2(c). In sharp contrast to the pure $Sr_4Ru_3O_{10}$ bulk or nanosheets, where two resistive anomalies at T_C and T_M were observed [6,13] [see also in the inset of Fig. 2(b)], here only one anomaly at T_C can be identified. These results suggest that the slightly Fe doping has less impact on the FM transition at T_C, but it suppresses the second magnetic transition at T_M completely.

C. Magnetoresistance of nanosheet

Figure 3 shows the *H*-dependent *R* at various temperatures obtained in a 12-nm-thick $Sr_4(Ru_{1-x}Fe_x)_3O_{10}$ ($x = 0.01$) nanosheet with *H* applied parallel to the *ab* plane [Fig. 3(a)] and the *c* axis [Fig. 3(b)]. Other $Sr_4(Ru_{1-x}Fe_x)_3O_{10}$ ($x = 0.01$) nanosheets exhibit very similar *R-H* properties as that of the 12 nm-thick sample. As we reported previously in pure $Sr_4Ru_3O_{10}$ nanosheets [14,16], the *R-H* curves with $H \| ab$ plane would present a "cusp"-shaped negative magnetoresistance (MR) above T_M, then transform dramatically into a "valley" behavior with a positive MR below T_M due to the reorientation of magnetic moments from an in-plane FM order to *c* axis [see also in Fig. 4(a)]. Unexpectedly, this phenomenon is not seen in the $Sr_4(Ru_{1-x}Fe_x)_3O_{10}$ ($x = 0.01$) nanosheet, where only "cusp"-shaped *R-H* curves with negative MR effect are observed down to 2 K when $H \| ab$ plane [Fig. 3(a)]. Interestingly, when the direction of the applied magnetic field is changed to the *c* direction ($H \| c$), the *R-H* curves present a "valley" shape in the whole *T*-range below T_C as shown in Fig. 3(b), significantly different to that observed in the pure $Sr_4Ru_3O_{10}$ nanosheet [Fig. 4(b)].

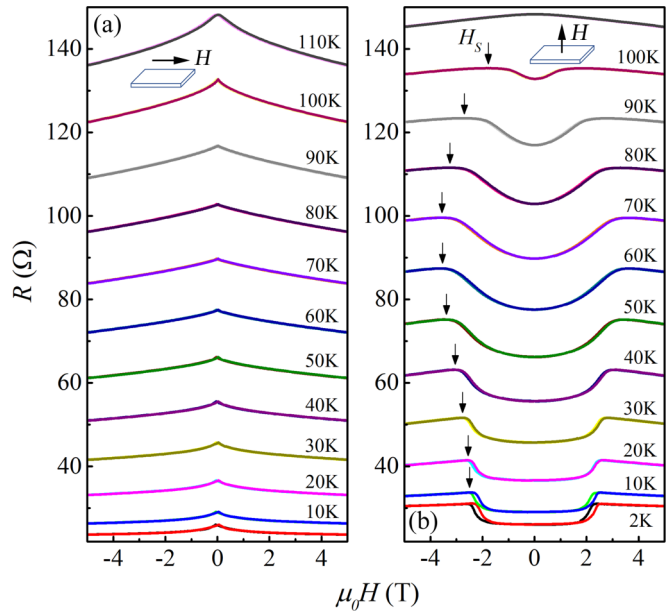

FIG. 3. Temperature dependent *R-H* properties of a 12-nm-thick $Sr_4(Ru_{1-x}Fe_x)_3O_{10}$ ($x = 0.01$) nanosheet for (a) $H \| ab$ and (b) $H \| c$, respectively. Arrows indicate the saturation field H_S of the resistance.

We have also measured the temperature dependence of *R-H* properties with $H \| ab$ and $H \| c$, respectively, of the $Sr_4(Ru_{1-x}Fe_x)_3O_{10}$ ($x = 0.01$) bulk single crystal (data not shown), the results are very similar to those observed in the nanosheet. The main difference is that the saturation field H_S [as indicated in Fig. 3(b)] with $H \| c$ in the bulk is much smaller than that in the nanosheet. For example, the H_S at 2 K in the bulk is ∼1.2 T; however, it increases to ∼2.5 T in the 12-nm-thick nanosheet [Fig. 3(b)]. This difference indicates that, similar to the pure $Sr_4Ru_3O_{10}$ [14,16], the shape

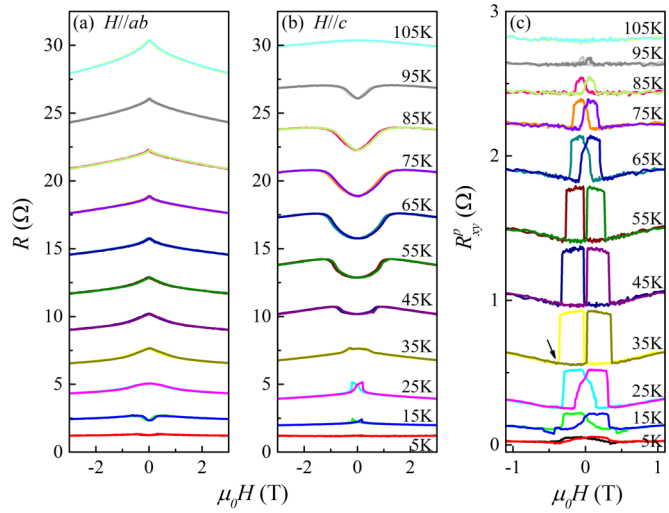

FIG. 4. Temperature-dependent *R-H* properties of a 34-nm-thick pure $Sr_4Ru_3O_{10}$ nanosheet for (a) $H \| ab$ and (b) $H \| c$, respectively. T_M of this sample is about 25 K. (c) Planar Hall effect of a 34-nm-thick $Sr_4Ru_3O_{10}$ nanosheet. *H* is aligned near the direction of the applied current, i.e., the [100] direction. Data is shifted vertically for clarity.

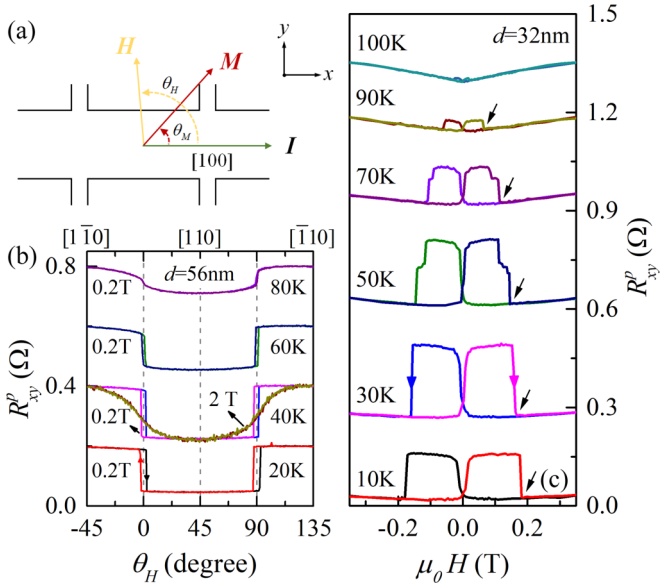

FIG. 5. (a) Sketch of the relative orientations of the applied current I, the external field H, and the in-plane magnetization M of the PHE measurement. (b) $R^p{}_{xy}-\theta_H$ curves measured at different temperatures in a 56-nm-thick $Sr_4(Ru_{1-x}Fe_x)_3O_{10}$ ($x = 0.01$) nanosheet. (c) Temperature dependent $R^p{}_{xy}-H$ curves measured with H applied about 10° off the [100] direction in a 32-nm-thick $Sr_4(Ru_{1-x}Fe_x)_3O_{10}$ ($x = 0.01$) nanosheet. Curves in panels (b) and (c) have been shifted vertically for clarity.

anisotropy in $Sr_4(Ru_{1-x}Fe_x)_3O_{10}$ ($x = 0.01$) still favors spins aligned in the *ab* plane.

The above results clearly demonstrate that the easy axis of magnetization is in the *ab* plane in the whole temperature range below T_C, and the second transition at T_M, which occurs in the pure $Sr_4Ru_3O_{10}$ bulk or nanosheets, has been fully suppressed in the $Sr_4(Ru_{1-x}Fe_x)_3O_{10}$ ($x = 0.01$) due to the lack of spin rotation from the *ab* plane to *c* direction. We would like to point out here that "disorder effect" induced by Fe-doping might be another reason for the suppression of the second transition. Disorders such as Fe will usually destroy the magnetic order and weak the intrinsic magnetism. However, both the magnetization [Figs. 1(b) and 1(c)] and the *R*-*H* properties show clearly that the Fe-doping here does not weaken the magnetism, but changes the easy magnetic direction from the *c* axis to *ab* plane, which strongly suggests the "disorder effect" can be excluded. Since the second transition at T_M is closely related to the competition between shape anisotropy and magnetocrystalline anisotropy in the pure $Sr_4Ru_3O_{10}$ nanosheets [14,16], the Fe-doping caused shrinkage of the *c* axis likely results in a suppression of the magnetocrystalline anisotropy so that it is insufficient to make the in-plane FM order of $Sr_4(Ru_{1-x}Fe_x)_3O_{10}$ ($x = 0.01$) switching back to the *c* direction.

D. Planar Hall effect of nanosheet

To assure the conclusion mentioned above, we further probed the in-plane magnetic property by means of planar Hall effect (PHE) [14,15]. The schematic diagram of the PHE measurement is shown in Fig. 5(a), where the current I is injected along the [100] crystal direction (i.e., x axis), and the magnetic field H is applied in the *ab* plane (i.e., x-y plane) with an angle of θ_H towards [100]. In this configuration, the planar Hall resistance, $R^p{}_{xy}$, can be written as [21]

$$R^p{}_{xy} = \frac{k}{d}M^2 \sin 2\theta_M, \tag{1}$$

where k is a coefficient related to the anisotropic MR, M is the in-plane magnetization, and θ_M is the angle between M and I.

Figure 5(b) shows the $R^p{}_{xy}-\theta_H$ curves obtained in a 56-nm-thick $Sr_4(Ru_{1-x}Fe_x)_3O_{10}$ ($x = 0.01$) nanosheet at different temperatures. When a magnetic field that is higher than the saturation field of the in-plane M, such as 2 T as representatively shown in Fig. 5(b), is applied, the $R^p{}_{xy}-\theta_H$ curve presents a sinusoidal-shaped twofold symmetry as predicted in Eq. (1) with extremes along ⟨110⟩ directions, due to the magnetization is fully polarized by the external magnetic field, i.e., $\theta_M \sim \theta_H$. Interestingly, when the field is decreased to 0.2 T, the $R^p{}_{xy}-\theta_H$ curves at different temperatures change into a square-wave form with twofold symmetry, accompanied by clearly hysteresis near all ⟨100⟩ directions, indicating that the magnetic polarization no longer linearly follows the external magnetic field, i.e., $\theta_M \neq \theta_H$. The above results suggest that the in-plane FM order in the $Sr_4(Ru_{1-x}Fe_x)_3O_{10}$ ($x = 0.01$) nanosheet at different temperatures is strongly anisotropic, and the easy axis of the magnetization is along the ⟨110⟩ directions. Since this magnetic anisotropy is almost the same as that of the pure $Sr_4Ru_3O_{10}$ nanosheet [14], we conclude that the present doping amount of Fe does not change the in-plane magnetic anisotropy of $Sr_4Ru_3O_{10}$.

Under this in-plane magnetic anisotropy, "spin-valve"-like switching in $R^p{}_{xy}$ with sweeping H is expected due to the flop of the in-plane magnetization between the easy magnetization directions (i.e., ⟨110⟩) [14]. This behavior is demonstrated in Fig. 5(c), which is obtained in a 32 nm-thick sample with an in-plane H aligned ∼10° off the [100] direction. It is clear seen that $Sr_4(Ru_{1-x}Fe_x)_3O_{10}$ ($x = 0.01$) nanosheet presents two significant features: (1) the $R^p{}_{xy}$ switching keeps sharp over the entire low temperatures; (2) the turn-off magnetic field (indicated as black arrows) of the switching increases continuously as the decrease of temperatures. These results are in sharp contrast to that observed in the pure $Sr_4Ru_3O_{10}$ nanosheet [Fig. 4(c)], where the $R^p{}_{xy}$ switching would gradually blur at temperatures below T_M, accompanied by a decrease of the turn-off magnetic field, due to there is a spontaneous spin-rotation process from the *ab* plane to the out-of-plane [14]. These differences indicate that Fe-doping is conducive to retain the magnetic moment in the *ab* plane.

E. Hall effect of nanosheet

As the Fe-doping gives rise to a complete in-plane FM order, an interesting question is whether the metamagnetic transition survives without the second transition at T_M when the magnetic field is along the *c* direction in the nanosheet. This is because the metamagnetic transition in the pure system was usually considered to be closely related to the second transition previously [8,11]. To answer this question, we performed Hall effect measurements on $Sr_4(Ru_{1-x}Fe_x)_3O_{10}$ ($x = 0.01$) nanosheets. For a FM sample, both the ordinary

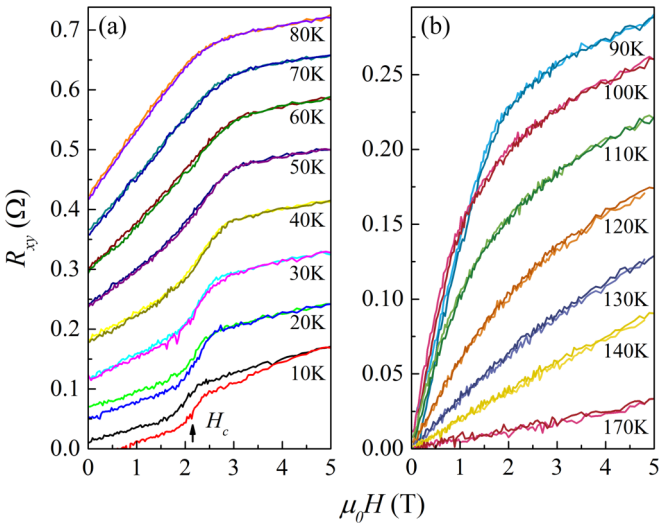

FIG. 6. Hall resistance R_{xy} of a 12-nm-thick $Sr_4(Ru_{1-x}Fe_x)_3O_{10}$ ($x = 0.01$) nanosheet as a function of perpendicular magnetic field H at various temperatures. Data in (a) has been shifted vertically for clarity.

Hall effect (OHE) and anomalous Hall effect (AHE) contribute to the Hall effect, the total Hall resistance R_{xy} can be empirically expressed as [22]

$$R_{xy} = R_0 H/d + R_s M_0(H, T)/d, \tag{2}$$

where R_0 and R_s are, respectively, the ordinary Hall coefficient and anomalous Hall coefficient, and M_0 is the magnetization, which depends on both the temperature T and the magnetic field H. Therefore, the anomalous Hall component, i.e., the second term in Eq. (2), can directly reflect the magnetization characteristics of a FM sample with $H \| c$.

Figure 6 shows the H-dependent Hall resistance R_{xy} of a 12-nm-thick $Sr_4(Ru_{1-x}Fe_x)_3O_{10}$ ($x = 0.01$) nanosheet measured at various temperatures. To see clearly, the data obtained in the temperature range of 10–80 K are shifted vertically and plotted in Fig. 6(a). All the R_{xy}-H curves can be described by Eq. (2) as expected. At $T > 140$ K [Fig. 6(b)], only a linear H dependence of R_{xy} caused by OHE is observed. With decreasing T from 140 K, the AHE gradually appears and become dominants the R_{xy} due to the FM transition, characterized by the 'knee' profile of the R_{xy}-H curve as shown in Fig. 6. In 50 K $< T <$ 100 K, the R_{xy}, which is proportional to the magnetization M_0, increases almost linearly below the saturation field with increasing H. However, at $T < 50$ K, a rapid increase of R_{xy} that reasonably originates from a rapid increase of M_0 in the vicinity of the saturation field is observed [see H_c indicated in Fig. 6(a)]. This property is very similar to the metamagnetic transition that has been observed for $H \| ab$ below T_M in the pure $Sr_4Ru_3O_{10}$ bulk [5] and the M-H behavior for $H \| c$ of the $Sr_4(Ru_{1-x}Fe_x)_3O_{10}$ ($x = 0.01$) bulk [inset of Fig. 1(b)].

We interpret the metamagnetic transition in the $Sr_4(Ru_{1-x}Fe_x)_3O_{10}$ ($x = 0.01$) for $H \| c$ as follows. At 50 K $< T < T_C$, the magnetic moments in the $Sr_4(Ru_{1-x}Fe_x)_3O_{10}$ ($x = 0.01$) at the ground state are FM-aligned in the ab plane but collectively rotate to the c direction with increasing the perpendicular H; at $T < 50$ K, however, the magnetic moments have been, at least partially, locked into the ab plane for $H < H_c$, and then change their direction to the c axis for $H > H_c$. This picture is supported by the observation of the MR effect shown in Fig. 3(b), where one can see that the "valley" below 50 K gradually changes from a "V"-like shape to a "U"-like shape with clear hysteresis near the saturation field H_S at low temperatures. Since the MR effect below the critical field $H_c \sim 2$ T shown in Fig. 3(b) mainly arises from spin scattering, the fact that the MR is almost independent of the perpendicular H at low temperatures indicates spins are indeed likely locked into the in-plane easy axis, i.e., ⟨110⟩ directions, for $H < H_c$. The observation of metamagnetic transition in $Sr_4(Ru_{1-x}Fe_x)_3O_{10}$ ($x = 0.01$) with $H \| c$ below 50 K clearly suggests that the metamagnetic transition itself in the $Sr_4Ru_3O_{10}$ system is actually less dependent on the second magnetic transition at T_M, but in fact, closely rely on the spin orientation.

IV. SUMMARY

We have investigated the magnetic property of $Sr_4(Ru_{1-x}Fe_x)_3O_{10}$ ($x = 0.01$). Results show that the second magnetic transition that observed in pure $Sr_4Ru_3O_{10}$ bulk or nanosheets is completely suppressed by Fe-doping, and the FM order (along ⟨110⟩ directions) remains in the ab plane in the whole temperature range below T_C, which is contrasted with that in pure bulk or nanosheet, where the FM order is mostly along the c direction at low temperatures. This finding clearly demonstrates that the second magnetic transition in $Sr_4Ru_3O_{10}$ is a result of the rearrangement of magnetic moments.

ACKNOWLEDGMENTS

The authors thank Prof. Lei Zhang in High Magnetic Field Laboratory (Hefei) for help in x-ray diffraction measurements. This work was supported by the National Natural Science Foundation of China (Grants No. 11674323, No. 11804297, No. 11774352, No. 11774305, and No. U1832214), the China Postdoctoral Science Foundation funded project (Grant No. 2018M632445), the International Users of Hefei Science Center of CAS (Grant No. 2016HSC-IU009), and the CAS/SAFEA international partnership program for creative research teams of China. The single crystal growth effort at Tulane was supported by the US Department of Energy under EPSCoR Grant No. DE-SC0012432 with additional support from the Louisiana Board of Regents.

[1] A. P. Mackenzie and Y. Maeno, Rev. Mod. Phys. **75**, 657 (2003).

[2] S. A. Grigera, R. S. Perry, A. J. Schofield, M. Chiao, S. R. Julian, G. G. Lonzarich, S. I. Ikeda, Y. Maeno,

A. J. Millis, and A. P. Mackenzie, Science **294**, 329 (2001).
[3] G. Koster, L. Klein, W. Siemons, G. Rijnders, J. S. Dodge, C.-B. Eom, D. H. A. Blank, and M. R. Beasley, Rev. Mod. Phys. **84**, 253 (2012).
[4] M. K. Crawford, R. L. Harlow, W. Marshall, Z. Li, G. Cao, R. L. Lindstrom, Q. Huang, and J. W. Lynn, Phys. Rev. B **65**, 214412 (2002).
[5] G. Cao, L. Balicas, W. H. Song, Y. P. Sun, Y. Xin, V. A. Bondarenko, J. W. Brill, S. Parkin, and X. N. Lin, Phys. Rev. B **68**, 174409 (2003).
[6] Z. A. Xu, X. F. Xu, R. S. Freitas, Z. Y. Long, M. Zhou, D. Fobes, M. H. Fang, P. Schiffer, Z. Q. Mao, and Y. Liu, Phys. Rev. B **76**, 094405 (2007).
[7] E. Carleschi, B. P. Doyle, R. Fittipaldi, V. Granata, A. M. Strydom, M. Cuoco, and A. Vecchione, Phys. Rev. B **90**, 205120 (2014).
[8] R. Gupta, M. Kim, H. Barath, S. L. Cooper, and G. Cao, Phys. Rev. Lett. **96**, 067004 (2006).
[9] X. N. Lin, V. A. Bondarenko, G. Cao, and J. W. Brill, Solid State Commun. **130**, 151 (2004).
[10] Y. J. Jo, L. Balicas, N. Kikugawa, E. S. Choi, K. Storr, M. Zhou, and Z. Q. Mao, Phys. Rev. B **75**, 094413 (2007).
[11] V. Granata, L. Capogna, M. Reehuis, R. Fittipaldi, B. Ouladdiaf, S. Pace, M. Cuoco, and A. Vecchione, J. Phys.: Condens. Matter **25**, 056004 (2013).
[12] M. Zhu, P. G. Li, Y. Wang, H. B. Cao, W. Tian, H. D. Zhang, B. D. Phelan, Z. Q. Mao, and X. Ke, Sci. Rep. **8**, 3914 (2018).
[13] Y. Liu, J. Y. Yang, W. K. Wang, H. F. Du, W. Ning, L. S. Ling, W. Tong, Z. Qu, Z. R. Yang, M. L. Tian, G. Cao, and Y. H. Zhang, New. J. Phys. **18**, 053019 (2016).
[14] Y. Liu, J. Y. Yang, W. K. Wang, H. F. Du, W. Ning, L. S. Ling, W. Tong, Z. Qu, G. Cao, Y. H. Zhang, and M. L. Tian, Phys. Rev. B **95**, 161103(R) (2017).
[15] Y. Liu, J. Y. Yang, W. W. Chu, H. F. Du, W. Ning, L. S. Ling, W. Tong, Z. Qu, G. Cao, Y. H. Zhang, and M. L. Tian, Appl. Phys. Lett. **111**, 033103 (2017).
[16] Y. Liu, W. W. Chu, J. Y. Yang, G. Q. Liu, H. F. Du, W. Ning, L. S. Ling, W. Tong, Z. Qu, G. Cao, Z. A. Xu, and M. L. Tian, Phys. Rev. B **98**, 024425 (2018).
[17] W. Schottenhamel, M. Abdel-Hafiez, R. Fittipaldi, V. Granata, A. Vecchione, M. Hücker, A. U. B. Wolter, and B. Büchner, Phys. Rev. B **94**, 155154 (2016).
[18] M. Zhou, J. Hooper, D. Fobes, Z. Q. Mao, V. Golub, and C. J. O'Connor, Mater. Res. Bull. **40**, 942 (2005).
[19] R. D. Shannon, Acta Cryst. **A32**, 751 (1976).
[20] S. I. Ikeda, Y. Maeno, S. Nakatsuji, M. Kosaka, and Y. Uwatoko, Phys. Rev. B **62**, R6089 (2000).
[21] K. Okamoto, J. Magn. Magn. Mater. **35**, 353 (1983).
[22] N. Nagaosa, J. Sinova, S. Onoda, A. H. MacDonald, and N. P. Ong, Rev. Mod. Phys. **82**, 1539 (2010).